Journal of Luminescence 261 (2023) 119915

Contents lists available at ScienceDirect

Journal of Luminescence

journal homepage: www.elsevier.com/locate/jlumin

Full Length Article

Efficient $CsPbBr_3$ sky-blue perovskite light-emitting devices Co-regulated by dual polymer additives

Li Song [a,*], Xiwei Guo [a], Yuan Liu [a], Yu Wen [a], Yingze Ren [a], Chang Tan [a], Meng Zhang [a], Hao Xu [a], Xiaoyang Guo [b,**], Lishuang Wang [c]

[a] State Key Laboratory of Reliability and Intelligence of Electrical Equipment, Tianjin Key Laboratory of Electronic Materials and Devices, School of Electronics and Information Engineering, Hebei University of Technology, Tianjin, 300401, PR China

[b] State Key Laboratory of Luminescence and Applications, Changchun Institute of Optics, Fine Mechanics and Physics, Chinese Academy of Sciences, Changchun, 130033, China

[c] State Key Laboratory of Featured Metal Materials and Life-cycle Safety for Composite Structures, School of Resources, Environment and Materials, Guangxi University, Nanning, Guangxi, 530004, China

ARTICLE INFO

Keywords:
Polymer additive
Sky-blue PeLED
Cs_4PbBr_6
Interface induction
Low dimensional
$CsPbBr_3$

ABSTRACT

Metal halide perovskite has aroused broad interests in fabricating colorful electroluminescent devices towards solid-state lighting and display technologies. However, blue perovskite light-emitting devices (PeLEDs) still face thorny problems such as poor working stability, low efficiency, and spectral instability. Here, we exploit a synergistic regulation on the crystallization and growth of pure bromide perovskite through interface inducing and polymer spatial confinement strategy to achieve blue emission. It is found that the ethanolamine modified PEDOT:PSS could induce low-dimensional Cs_4PbBr_6:$CsPbBr_3$ composite. Polyvinyl pyrrolidone (PVP) together with poly ethylene glycol (PEG) additives inhibited its coalescence and ripening and passivated the defects simultaneously. As a consequence, dual-polymer regulated Cs_4PbBr_6:$CsPbBr_3$ PeLEDs presented an external quantum efficiency (EQE) of 3.73% and maximum brightness of 7051 cd/m^2. Our facile method may provide alternative approaches to construct efficient blue PeLEDs.

1. Introduction

As one of the three primary colors, blue electric-drive light-emitting devices (LEDs) play a pivotal role in solid-state lighting and full-color displays [1–4]. Metal halide perovskites are regarded as potential alternatives in these areas due to its intrinsic high PLQY, narrow bandwidth and tunable energy bandgap [5,6]. The past few years have witnessed the booming development of perovskite LEDs (PeLEDs) with external quantum efficiency soaring up to 22.2% for NIR LEDs and 28.1% for green LEDs [7–10]. Great efforts have also been made to improve the electroluminescent performance of blue PeLEDs through cation/anion doping or constructing quasi-two dimensional structure [11–19]. However, their comprehensive performance is still lag behind the green and red counterparts. Novel strategies to manipulate the blue perovskite emission layer are still in urgent necessity to develop perovskite LEDs with high brightness and efficiency.

Generally, there are two strategies to construct blue perovskite films including the chemical composition adjustment and quantum-well low dimensional structure modulated by long-chain spacer. The mixed Cl/Br halides perovskites often suffer from phase separation originated from ion migration, facing the undesirable spectra instability stimulated by external conditions such as applied voltage bias or UV light excitation [20–22]. For the long-chain organic ligand incorporated quasi-two dimensional pure bromide perovskites, the thickness of quantum-well which often denote as n need to be limited below 5 to keep the wavelength in the blue region [23,24]. To realize the low n phase, more long-chain ligands even extra ligands are required to be introduced in the precursor, which will in turn reduce the conductivity of the film. In addition, the quasi-2D perovskite films are composed of different n phases. The small n component tends to undergo coalescence and ripening upon annealing, shifting the spectra peak to longer wavelength [24]. Similar to the long-chain organic spacer, inorganic spacer may be a potential alternative to construct low dimensional perovskite films. This strategy has been demonstrated in Cs–Pb–Br perovskite system in which

* Corresponding author.
** Corresponding author.
E-mail addresses: songli@hebut.edu.cn (L. Song), guoxy@ciomp.ac.cn (X. Guo).

https://doi.org/10.1016/j.jlumin.2023.119915
Received 22 March 2023; Received in revised form 7 May 2023; Accepted 10 May 2023
Available online 16 May 2023

the large bandgap Cs_4PbBr_6 spaced $CsPbBr_3$ [25]. The Cs_4PbBr_6:$CsPbBr_3$ composite exhibited tunable wavelength from green region (~520 nm) to pure blue region (<480 nm) under the triggeration of water or amino alcohol [25,26]. It is also found that the hydroxy-rich NiO_x could also induce the formation of Cs_4PbBr_6 and then form the blue emissive Cs_4PbBr_6:$CsPbBr_3$ phase [27]. However, the reported Cs_4PbBr_6:$CsPbBr_3$ nanocomposites either suffered from poor morphology or low PLQY, resulting in the limited EL performance. Strategies to improve the performance of PeLED based on the blue Cs_4PbBr_6:$CsPbBr_3$ are still necessary.

From the perspective of crystallization and growth of the perovskite films, polymers additives with natural skeletons can theoretically control the growth of crystal. Some polymers such as aromatic polyimide (PIP) [28], poly (ethylene oxide) [29] and poly (ethylene glycol) (PEG) [9,30] have been adopted to confine the crystals' growth space, achieving remarkably reduced nanocrystal size and smoother surface morphology. Therefore, the combination between polymer and Cs_4PbBr_6:$CsPbBr_3$ may generate a blue emissive perovskite film with superior optical and electrical properties. Whereas, the critical role of different polymer species on the crystallization of Cs_4PbBr_6:$CsPbBr_3$ and their impact on the physical characteristics of perovskite has not been fully explored.

Herein, an interface inducing strategy through introduction of ethanolamine (EA) into PEDOT:PSS was employed to control the crystallization of CsBr-rich perovskite precursor. The EA could trigger the formation of Cs_4PbBr_6 and then spatially confined the growth of $CsPbBr_3$, resulting in mixed LD/3D perovskite phases. The space confinement of the different polymer additives was also investigated. It is found that the 3D could be completely diminished after the introduction of polyvinyl pyrrolidone (PVP). While the PEG could not effectively inhabit the growth of LD phase, the PLQY was improved due to the passivation effect of uncoordinated Pb^{2+} originating from the C–O–C functional group. By further allying the PVP with PEG, an ultrasmooth perovskite film with peak wavelength located at 483 nm was obtained. The corresponding dual-polymers tailored sky-blue PeLED exhibited maximum brightness of 7051 cd/m^2, maximum current efficiency of 5.41 cd/A and EQE of 3.73%, which is 2.7 times higher than the single PVP additive regulated PeLEDs. Our results would shed light on the regulation of crystallization and growth of the pure bromide based all-inorganic perovskite to achieve efficient blue PeLEDs.

2. Experimental section

2.1. Materials

Poly (3,4-ethylenedioxythiophene)-poly (styrene sulfonate) (PEDOT:PSS, Clevios AI4083, Xi'an Polymer Light Technology Co.), $PbBr_2$ (99.9%, Youxuan New Energy Technology Co.) and 1,3,5-tris (2-N-phenylbenzimidazolyl)-benzene (TPBi, Xi'an Polymer Light Technology Co.), CsBr (99.9%, Kanto Chemical. Co., Inc.), Lithium Fluoride (LiF, Aladdin, 99.99%), PEG (Mw = 200,000, Aladdin) and PVP (Mw = 1,300,000, Aladdin), Ethanolamine (EA, 99%, Innochem). All materials were used as original without any purification.

2.2. Film fabrication and characterization

The EA first dissolved in ethanol with desired weight ratio (100, 200 and 300 mg/mL) and the blended with PEDOT:PSS in a volume ratio of 1:10. CsBr and $PbBr_2$ (65 mg/80 mg for molar ratio of 1.4, 69 mg/76 mg for molar ratio of 1.59 and 75 mg/70 mg for molar ratio of 1.86) was mixed in 1 mL DMSO and then rigorously stirred at 50 °C to form transparent perovskite precursor. The polymer additives were dissolved in DMSO with a weight ratio of 10 mg/mL and blended with the perovskite precursor in a volume ratio of 1:10 before use. The perovskite films were spin-coated on the ITO/PEDOT:PSS substrates or quartz substrates with a speed of 4500 rpm for 60 s and then annealed at 70 °C for 5 min. For the thermally evaporated perovskite film, six pairs of CsBr (11 nm) and $PbBr_2$ (3 nm) were alternatively deposited on either PEDOT:PSS or PEDOT:PSS-EA modified quartz substates and annealed at 110 °C for 30 min. Film morphology was characterized by AFM (Shimadzu SPA-9700) and scanning electron microscope (SEM, Hitachi S-4800). Fluorescence spectra were collected by a fiber spectrometer (AvaSpec-ULS2048L) with an excitation wavelength of 365 nm. Time-resolved PL spectra were analyzed by Edinburgh FLS920 spectrometer. Absorption spectra of perovskite film were characterized by Persee T6 UV–Vis spectrometer. The XRD patterns of perovskite film were carried out by Bruker Advance D8 X-ray diffractometer. The FTIR was measured on a Thermo-Nicole iS50 FTIR-spectrometer. For TA measurements, a laser beam (800 nm, pulse width 40 fs, 1 kHz, 5 W) was first split into two beams through a 5:5 beam splitter. One was used to generate the pump light via passing through a BBO frequency doubling crystal and the other was focused into CaF_2 to produce white detection light. The pump beam and probe beam were crossed at the perovskite sample with a beam spot of 200 μm. The transient absorption signal was gathered by the Ocean Optics spectrometer (HR4000). The ultraviolet photoelectron spectroscopy (UPS) was measured by using an ESCALAB 250Xi equipment with a monochromatized HeI (21.22 eV) excitation source. Transient PL decay and PLQY were performed on an Edinburgh FLS920 spectrometer coupled with an integrating sphere.

2.3. Device fabrication and characterization

The devices were prepared on precleaned ITO-coated transparent substrates. The ITO surface was ultrasonically cleaned with deionized water, ethanol and acetone solvents successively, and followed by the UV-ozone treatment for 20 min. Pure PEDOT:PSS or EA modified PEDOT:PSS was spin-coated on ITO substrates at 2500 rpm for 30 s and annealed at 140 °C for 20 min. After that, the substrates were transferred into a N_2 filled glove box for the following preparation of perovskite layers. Finally, the samples were transferred into a home-made vacuum chamber (QHV-R20) to thermally deposit the electron transport layer (TPBi, 40 nm), electron injection layer (LiF, 2 nm), and cathode (Al, 100 nm) under a pressure of below 4×10^{-4} Pa. The current density-voltage-luminance (J-V-L) curves were recorded using a Keithley 2400 source meter equipped with a luminance meter LS160. The EL spectra were acquired by AvaSpec-ULS2048L fiber spectrometer. A Lambertian emission profile was assumed for the calculation of EQE from the brightness, current, and EL spectrum. All measurements were performed in air with simple encapsulation by UV glue.

3. Results and discussions

Aiming at achieving blue-emission in pure bromide-based $CsPbBr_3$ with Cs_4PbBr_6 spacer, the Cs/Pb ratio in the precursor was critical to the crystallinity of the perovskite films. Therefore, we first investigated spectra evolution of the perovskite films towards different Cs/Pb ratios under the condition of EA induction. As shown in Fig. 1a, when at a relatively low Cs/Pb ratio of 1.4, the PL spectrum presented only one Gaussian shaped curve with peak centered at ~522 nm and full width at half maximum (FWHM) of ~16 nm. As the Cs/Pb gradually increased, a gradually slight blue shift in PL peak for the bulk perovskite phase (521 nm for Cs/Pb~1.59 and 515 nm for Cs/Pb~1.86) was observed which may arise from space confinement effect. The absorption spectra for the perovskite with different Cs/Pb ratios in Fig. 1b also showed a slightly blue-shifted onset band edge which suggested a widened bandgap and coincided well with the dominant PL peaks. In addition to the shift in the dominant peak, an extra peak appeared in the short wavelength region. And the newly emerged peak wavelength showed Cs/Pb-dependent behavior and achieved in the pure-blue region at Cs/Pb of 1.86:1, indicating that a low-dimensional $CsPbBr_3$ coexisted with the bulk phase. High-resolution transmission electron microscopy (HRTEM) (Fig. S1) also confirmed the coexistence of $CsPbBr_3$ and Cs_4PbBr_6. The

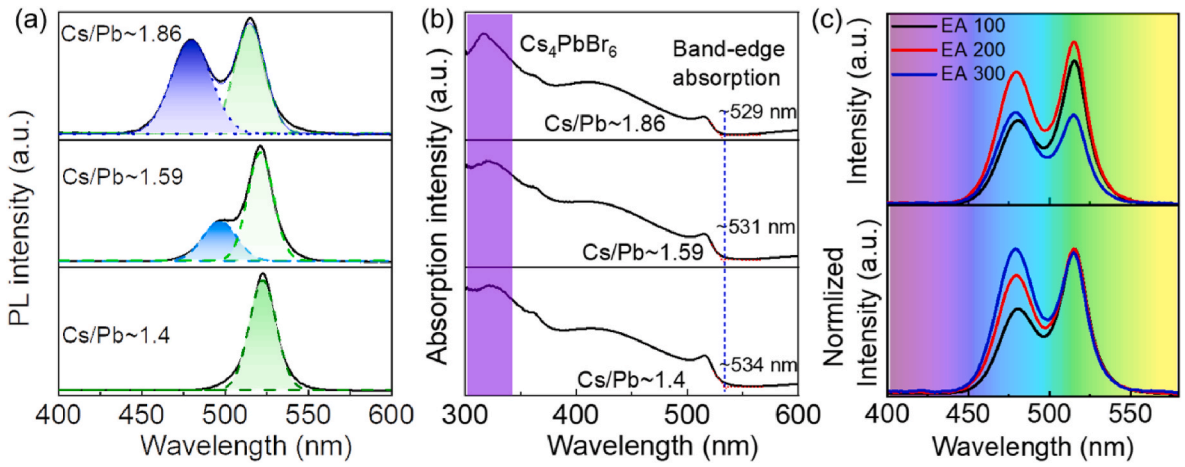

Fig. 1. (a) PL spectra and (b) absorption spectra for the perovskite films with different Cs/Pb molar ratios grown on EA-modified PEDOT:PSS (EA-200). (c) PL curves for the perovskite films (Cs/Pb = 1.86) formed on PEDOT:PSS doped with different EA concentrations.

double mixed peak wavelength indicated a non-completely energy transfer between these two phases. Note, the low-dimensional $CsPbBr_3$ depend not only on the Cs/Pb ratio but also on the buried EA-modified PEDOT:PSS. To uncover the function of EA, we here take the Cs/Pb = 1.86 as an example to investigate the spectra variation. As can be seen in Fig. 1c, the relative emission intensity of the low-dimensional phase at ~480 nm instead of its peak wavelength was dependent on the doping amount of the EA in PEDOT:PSS, suggesting that the EA did not alloy in the lattice as the bulk organic ligand to limit the growth of the $CsPbBr_3$ directly and did not form the spacer-dependent quasi-two dimensional perovskite phases [31]. The PL intensity reached the maximum when the doping concentration of EA was 200 mg/mL. The stronger absorption peak around 315 nm in UV spectra which corresponded to the bandgap energy of the Cs_4PbBr_6 phase at a higher Cs/Pb ratio also affirmed the coexistence of Cs_4PbBr_6 and $CsPbBr_3$. Therefore, the Cs/Pb-dependent peak wavelength and EA-dependent peak intensity phenomena confirmed that the EA directly induced the formation of wide-bandgap Cs_4PbBr_6 and then Cs_4PbBr_6 serve as a new spacer to restrict the growth of the $CsPbBr_3$, resulting in the blue emission in perovskite films. The thickness of the perovskite film is too thin to observe some weak diffraction signal, making almost no difference in the X-ray diffraction patterns to reveal the effect of EA on the perovskite crystal structure (Fig. S2). The induction role of EA was further verified by thermally evaporated perovskite films under CsBr-rich condition (Fig. S3), in which the absorption of Cs_4PbBr_6 and the X-ray diffraction intensity at 2 θ = 30.7 ° for Cs_4PbBr_6 in the EA-perovskite is much stronger than that of pristine perovskite. Fourier-transform infrared (FTIR) (Fig. S4) revealed that the characteristic –NH stretching vibration [32] at 3351 cm^{-1} and 3290 cm^{-1} covered with the broadband from 3000 to 3500 cm^{-1} which attributed to the –OH stretching vibration was weakened. At the same time, the absorption peak in the region of 1050–1090 cm^{-1} that was attributed to the scissoring vibration of the –OH group [33] exhibited a shift from 1076 to 1067 cm^{-1} after the addition of $CsPbBr_3$ into EA. These changes supported the interaction between EA and $CsPbBr_3$, promoting the formation of Cs_4PbBr_6 as the UV–vis absorption of the thermally deposited perovskite films demonstrated in Fig. S3.

It is well known that *in situ* perovskites' crystallization involved nucleation and following growth which are closely related to the buried substrates. AFM measurements were further adopted to investigate perovskites' crystallization on different EA-modified PEDOT:PSS. As seen in Fig. 2a, the perovskite film formed on the pristine PEDOT:PSS exhibited randomly distributed granular nanocrystals with many voids and root mean square (RMS) roughness achieving 16.95 nm. In comparison, when the EA was adopted, the voids in the films were reduced

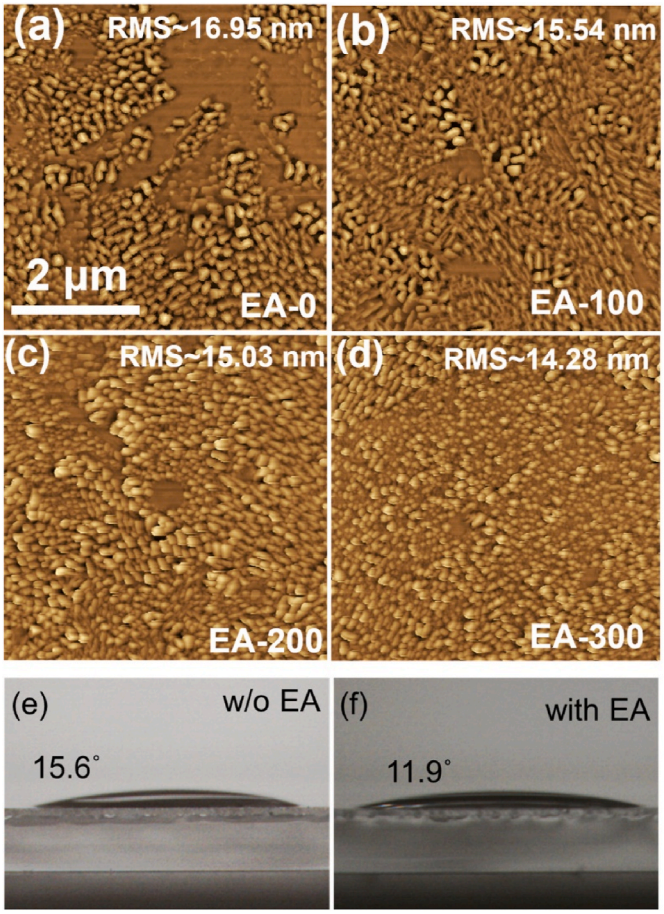

Fig. 2. (a)~(d) are the atomic force microscope (AFM) images of the perovskite films on different EA-modified PEDOT:PSS. Contact angle of DMSO on (e) pure PEDOT:PSS and (f) EA-PEDOT:PSS films.

and the crystal size was also decreased, resulting in flatter morphology (Fig. 2b–d). The decreased contact angle of perovskite precursor on EA-PEDOT:PSS (Fig. 2e and f) in comparison to that on neat PEDOT:PSS revealed that better wettability was achieved due to the functional amino and hydroxyl groups interfacial hydrogen bonding interactions. The more hydrophilic feature of EA-PEDOT:PSS would be beneficial to reduce the necessary free energy for heterogeneous nucleation and

increase the nucleation sites. This change in the morphology agreed well with previous reports [34,35].

Although EA can induce Cs_4PbBr_6 separated blue $CsPbBr_3$, the bulk phase cannot be suppressed completely, making the double phase coexisted perovskite films suffer from low color purity. Given that the polymeric additives may serve as a natural framework to limit the growth of crystals and maintain the perovskite with high color purity. We here select two common polymers, PVP and PEG, to further modulate the crystallinity and emission spectra. Fig. 3a and b showed the morphologies with PVP and PEG additives separately. Clearly, the PVP can actually inhibit the crystal growth and the tiny grains aggregated into an exceedingly smooth film with an RMS of 1.64 nm which was significantly reduced compared with the undoped perovskite film (Fig. 2c). Correspondingly, the sample showed a pure blue emission with peak wavelength at 480 nm and FWHM of 26.8 nm. As for the PEG additive, a completely opposite change in the film morphology was observed. Although the surface roughness was reduced to 13.35 nm, the crystal grains became larger with an average size of ~207 nm (Fig. S5) compared with that of the undoped perovskite film, denying its restriction role. As a result, the spectra for the PEG-regulated perovskite presented a multi-peak curve with a dominant peak at 517 nm, confirming that the PEG is unfavorable to the growth of the low-dimensional perovskite phase. Previous investigation demonstrated the C–O–C group would donate electron and interact with the uncoordinated Pb^{2+} [9,13], which may promote the crystallization of the perovskite into bulk phase competing with its own skeletal restraint. However, we note the PL intensity for the PEG-Cs-Pb-Br film was much higher than that without the PEG additive, demonstrating that PEG could passivate the nonradiative taps as the photograph shown in Fig. S6. Considering the restriction role of PVP and defect-passivation role of PEG, we conceived to manipulate the emission wavelength as well as the intensity by a combination of PEG and PVP in the precursor.

As shown in Fig. 3c, the dual polymer regulated film was filled with featureless grains, showing ultra-smooth surface morphology with an RMS of 1.25 nm. A single and strong sky-blue emission located at 483 nm with FWHM of 27 nm is achieved in the corresponding perovskite film. Meanwhile, the average PL lifetime was prolonged from 2.21 ns for PVP-perovskite to 3.67 ns for the PVP&PEG-perovskite film (Fig. S7), and PLQY was increased from 6.9% for PVP-perovskite to 13.4% for PVP&PEG-perovskite. Such results once again demonstrated the passivation role of PEG. The slight redshift in PL spectra after incorporating PEG may originate from the changed ratio of surface to bulk emission as previously reported [36]. To further reveal the carrier kinetics, we conducted transient absorption spectra of these films (Fig. 3g–i). The PVP-modulated perovskite showed a single bleach peak with the inhomogeneously broadened feature, indicating that the perovskite film consists of a collection of different nanosize grains. The indistinguishable bleach peaks indicate the bandgaps approached size independence for the LD multiphase perovskite nanocrystals [37,38]. In the PEG-modulated perovskite films, two bleach minimums were observed (Fig. 3h) corresponding the low-dimensional and bulk phase, which were in good agreement with the static PL spectrum. An evident energy transfer from 460 nm to 514 nm in the early 2 ps, in good line with the PL results. Similar to the phenomena observed in PVP-perovskite film, the PVP-PEG co-regulated films also exhibited a broad bleach peak, and a larger redshift in the bleach minimum has been observed compared with the PVP-$CsPbBr_3$, suggesting the crystal with many different size distributions, which agrees well with the broadened PL curve (Fig. 3i).

Based on the above experimental observations, we proposed a model for the formation of the blue emissive perovskite layer to clarify the role of EA and polymer additives (Fig. 4). Without EA, the perovskite film is inclined to grow into a bulk phase with excess CsBr. While for the case of introducing EA in PEDOT:PSS, its hydroxyl group bared on the PEDOT:

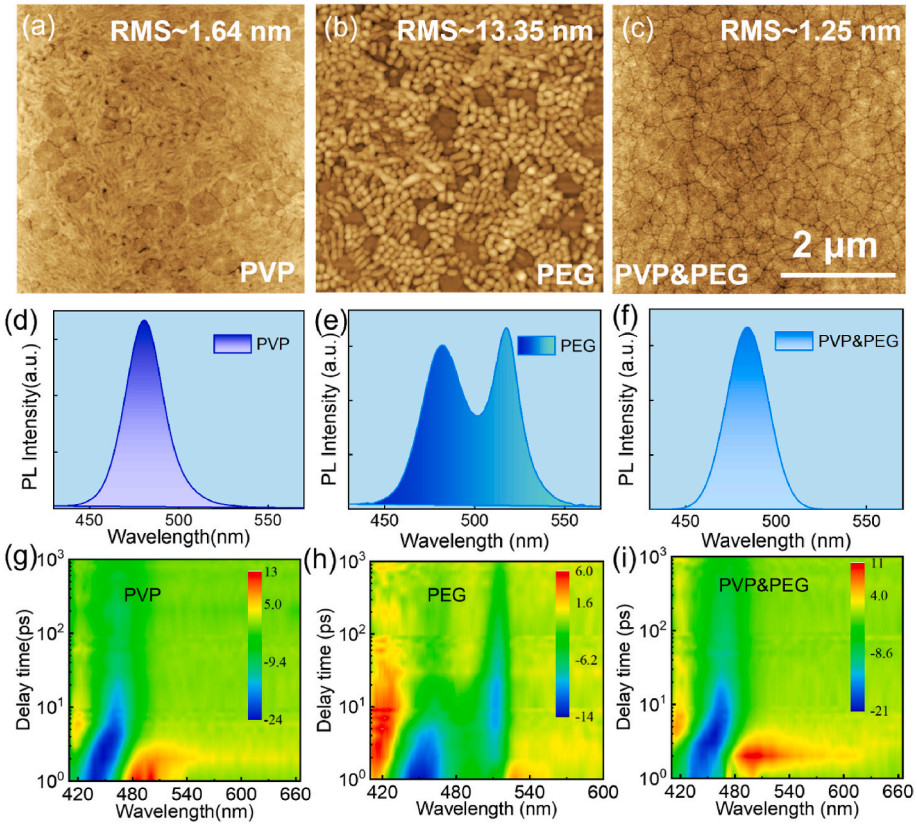

Fig. 3. AFM images for the perovskite formed on EA-PEDOT:PSS (EA200) with different polymer additives (a) PVP, (b) PEG, (c) PVP and PEG.(d)~(f) are the PL curves corresponding to (a)~(c). (g)~(i) are the corresponding transient absorption spectra.

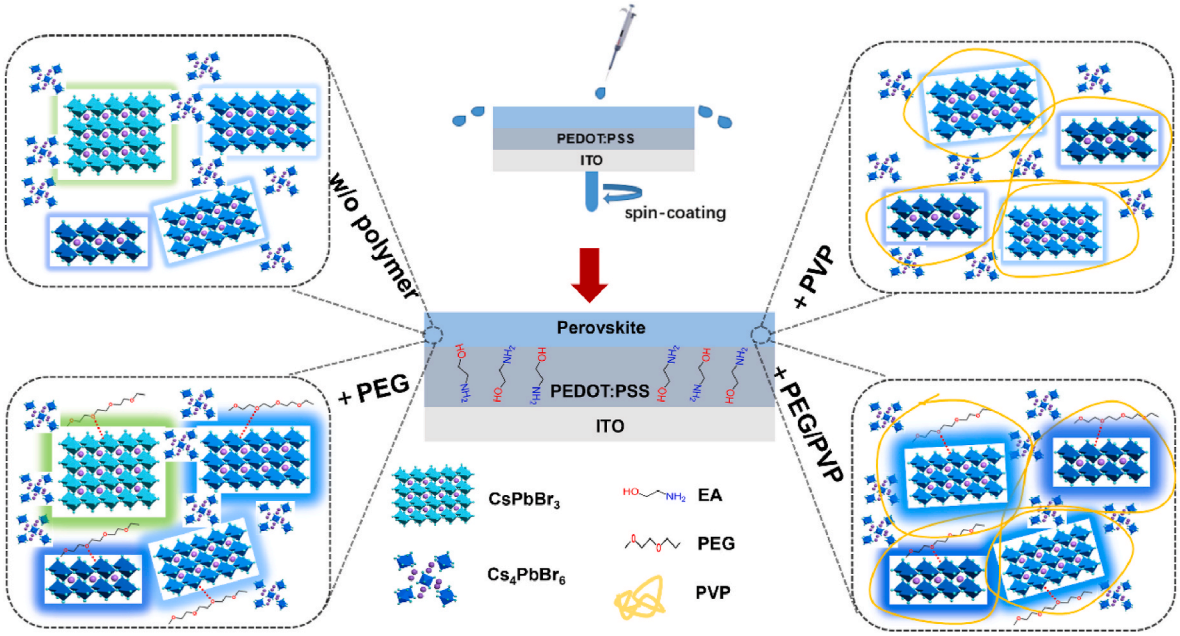

Fig. 4. A schematic depicting the crystallization process under the control of EA and polymer additives.

PSS surface interacted with the Br atoms, promoting the binding of CsBr and $CsPbBr_3$ and generating Cs_4PbBr_6. The emerging Cs_4PbBr_6 will spatially shrink the growth of partial $CsPbBr_3$ and result in the additional blue emissive LD phase. The PVP scaffold could increase the dispersion of the LD phase and synergistically limit its growth, making the bandgap pin at the blue region. The PEG network could passivate the nonradiative defects by coordinating with the unsaturated Pb^{2+} rather than act as a limiting scaffold. As a consequence, bright blue perovskite films were eventually obtained under synergistic control of the EA and dual polymer additives.

To explore the EL properties of EA and polymer-modulated blue or sky-blue perovskite films, PeLEDs with the configuration of ITO/PEDOT:PSS-EA/perovskites/TPBI/LiF/Al were further constructed. Detailed device structure and corresponding energy alignment were illustrated in Fig. S8, respectively. Note, the modification of PEDOT:PSS by EA not only played a critical role in triggeration of low-dimensional Cs_4PbBr_6:$CsPbBr_3$ composite but also increased PEDOT:PSS conductivity via promoting the connection of the conductive PEDOT chains and thus lead to a hole injection enhancement [32]. The optical-electrical performances of the PeLEDs with PVP-PEG dual polymers were shown in Fig. 5

Table 1
Summary of EL parameters of the PeLEDs with different polymer additives prepared on EA-PEDOT:PSS buried hole transport layer.

polymer	EL peak (nm)	L_{max} (cd/m^2)	Peak CE (cd/A)	EQE_{max} (%)	V_{on} (V)
PVP	484	2663	1.76	1.37	3.0
PEG	485/516	10,356	13.49	5.12	2.6
PVP&PEG	490	7051	5.41	3.73	2.8

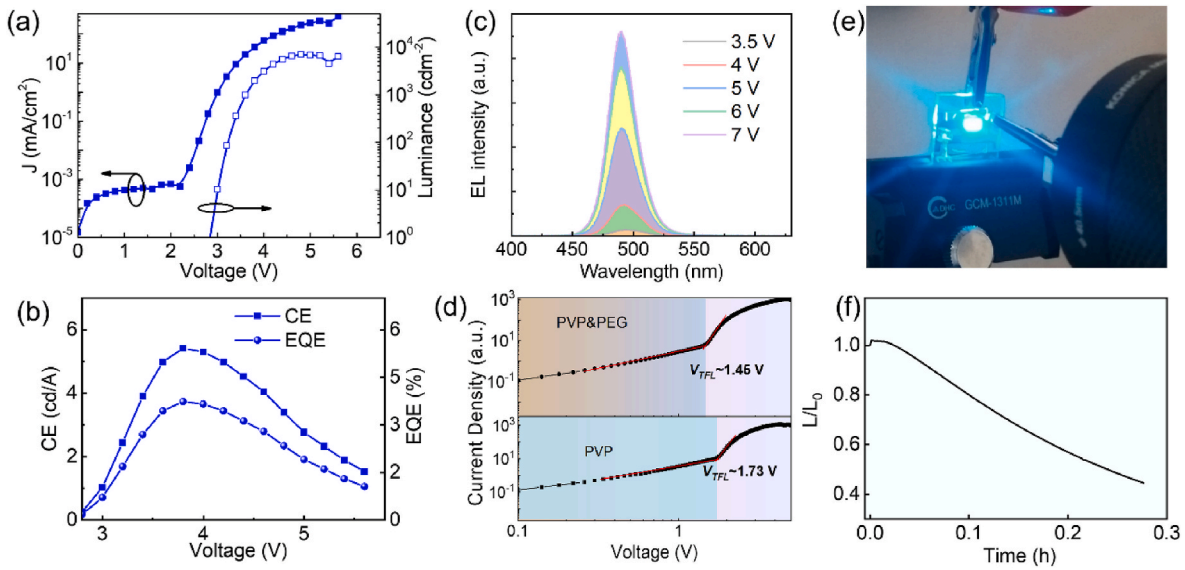

Fig. 5. EL characteristics for the PeLEDs (a) J-L-V curves (b) CE-V and EQE-V curves (c) EL spectra under different voltage biases, (d) SCLC curves of the perovskite films with PVP and PVP/PEG additives, respectively. (e) Photograph of the lightning devices. (f) Working stability for the PeLED under constant current with initial brightness of ~100 cd/m^2.

and summarized in Table 1. From the J-V-L curves (Fig. 5a), it can be seen that the device started to turn on at ~2.8 V and reached the brightest of 7051 cd/m^2 at about 4.8 V. The leakage current maintained at a low level below ~10^{-2} mA/cm^2 before the turn-on voltage due to the dense and smooth morphology. The device behaved a bright sky-blue emission with almost stable spectra at ~490 nm and FWHM of 26 nm as shown in Fig. 5c and e. The corresponding CIE coordinates are (0.07, 0.32). Though the EL spectra are about 6 nm redshifted compared with the PVP-regulated PeLEDs, the brightness and efficiency are about 2.7 times and 3.1 times higher than that with only the PVP additive (Table 1 and Fig. S9). The maximum current efficiency and EQE reached 5.41 cd/A and 3.73%, respectively. The improvement in current efficiency and brightness can be attributed to the reduction of hole-injection barrier between EA-PEDOT:PSS and perovskite layer (Fig. S10), as well as the defect passivation effect of PEG which can be verified by the reduced trap density calculated from the J-V curves of hole-only devices via space charge limited current (SCLC) model. As shown in Fig. 5d, the J-V curves for the hole-only devices (ITO/EA-PEDOT/perovskite/HAT-CN/Al) contains three different regions: Ohmic region at low voltage, trap-filled limited region with a sharp increase in current and SCLC region. The defect density (N_d) can be determined by the trap-filled limiting voltage (V_{TFL}) above which all the traps are anticipatedly to be filled using the equation of $N_d = 2\varepsilon\varepsilon_0 V_{TFL}/eL^2$ [18,39]. The $\varepsilon, \varepsilon_0$,e and L meant relative dielectric constant (16.46 for $CsPbBr_3$) [40], vacuum permittivity, elementary charge and film thickness, respectively. The calculated trap density for the PVP-PEG-$CsPbBr_3$ perovskite is 1.96 × 10^{18} cm^{-3}, which is lower than that of PVP-$CsPbBr_3$ film (1.66 × 10^{18} cm^{-3}), affirming the defect passivation effect from PEG. The working stability was measured under a constant current density at an initial luminance of 100 cd/m^2. The PeLEDs can survive 15 min (Fig. 5f). Though the comprehensive performance is still inferior to that of the best-reported sky-blue PeLED, it is worth noting that such performance is moderate among the reported pure-bromide all-inorganic $CsPbBr_3$ perovskite LEDs without any cation or halide alloying (Table S1). Both the intrinsic instability of the perovskite film and the defects that exited either in the grain boundaries or the interface imperfection may result in poor device stability. It is expected that the stability and optical performance of the blue PeLED would be significantly improved by further proper metal doping strategies [41,42].

4. Conclusion

In conclusion, we report a facile methodology to construct blue perovskite film in Cs–Pb–Br system levering the advantage of interface inducing effect and the polymer network. The ethanolamine-modified PEDOT:PSS could promote the formation of Cs_4PbBr_6 due to the interaction between OH and –NH_2 functional groups and perovskite. Cs_4PbBr_6 compressed the growth space for $CsPbBr_3$ and formed Cs_4PbBr_6 spaced low-dimensional $CsPbBr_3$. We further adopted polymer scaffold to further control the crystallization and growth process of the perovskite film. It is found that PVP and PEG polymer matrix play completely different roles. PVP could spatially inhibit the ripening of Cs_4PbBr_6:$CsPbBr_3$ upon thermal annealing and thus stabilize the spectra with narrow linewidth. Although PEG has little on effect on tuning the morphology and PL profile, the trap states can be well passivated with significantly enhance light emission originating from the interaction between C–O–C and Pb^{2+}. Combining the spatial confinement of PVP and defect passivation of PEG, we reached a sky-blue perovskite film with FWHM of 26 nm and peak wavelength at 490 nm. The corresponding sky-blue PeLEDs showed a moderate EL performance with a luminance of 7051 cd/m^2 and EQE of 3.73%. Our results disclosed that different polymers could have different effects on the morphology and optical properties of perovskites in the construction of Cs_4PbBr_6:$CsPbBr_3$ LD perovskites.

Author statement

Li Song conceived, designed the project, and wrote original draft. Xiwei Guo: contributed significantly to film fabrication and analysis. Yuan Liu optimized the device performance. Yu Wen, Yingze Ren, Chang Tan, Meng Zhang and Hao Xu performed optical characterization and analysis. Xiaoyang Gu and Lishuang Wang helped review and provide constructive discussion. All authors contributed to the writing of the manuscript and discussion of the results.

Declaration of competing interest

The authors declare that they have no known competing financial interests or personal relationships that could have appeared to influence the work reported in this paper.

Data availability

Data will be made available on request.

Acknowledgments

The authors wish to thank Dr Wei Wang for his assistance with contact angle measurement. This study was supported by the Foundation of Hebei Education Department (BJ2021017), S&T Program of Hebei (216Z0601G) and open foundation of State Key Laboratory of Featured Metal Materials and Life-cycle Safety for Composite Structures (Grant No. GXYSOF19).

Appendix A. Supplementary data

Supplementary data to this article can be found online at https://doi.org/10.1016/j.jlumin.2023.119915.

References

[1] Z. Xu, B.Z. Tang, Y. Wang, D.G. Ma, Recent advances in high performance blue organic light-emitting diodes based on fluorescence emitters, J. Mater. Chem. C 8 (2020) 2614–2642.
[2] L. Wang, Z. Zhao, G. Zhan, H. Fang, H. Yang, T. Huang, Y. Zhang, N. Jiang, L. Duan, Z. Liu, Z. Bian, Z. Lu, C. Huang, Deep-blue organic light-emitting diodes based on a doublet d–f transition cerium(III) complex with 100% exciton utilization efficiency, Light, Sci. Appl. 9 (2020) 157.
[3] Y. Kondo, K. Yoshiura, S. Kitera, H. Nishi, S. Oda, H. Gotoh, Y. Sasada, M. Yanai, T. Hatakeyama, Narrowband deep-blue organic light-emitting diode featuring an organoboron-based emitter, Nat. Photonics 13 (2019) 678.
[4] H. Xiang, R. Wang, J. Chen, F. Li, H. Zeng, Research progress of full electroluminescent white light-emitting diodes based on a single emissive layer, Light Sci. Appl. 10 (2021) 206.
[5] Y. Liu, F. Li, Q. Liu, Z. Xia, Synergetic effect of postsynthetic water treatment on the enhanced photoluminescence and stability of $CsPbX_3$ (X = Cl, Br, I) perovskite nanocrystals, Chem. Mater. 30 (2018) 6922–6929.
[6] B. Li, Y. Zhang, Y. Xu, Z. Xia, Design optimization of $CsPbBr_3$ nanocrystals into zeolite Beta composites as ultra-stable green emitters for backlight display applications, J. Mater. Chem. C 9 (2021) 12118–12123.
[7] Y. Miao, L. Cheng, W. Zou, L. Gu, J. Zhang, Q. Guo, Q. Peng, M. Xu, Y. He, S. Zhang, Y. Cao, R. Li, N. Wang, W. Huang, J. Wang, Microcavity top-emission perovskite light-emitting diodes, Light Sci. Appl. 9 (2020) 89.
[8] J.-W. Lee, N.-G. Park, Quasi-two-dimensional perovskite light emitting diodes for bright future, Light Sci. Appl. 10 (2021) 86.
[9] Z. Liu, W.D. Qiu, X.M. Peng, G.W. Sun, X.Y. Liu, D.H. Liu, Z.C. Li, F.R. He, C. Y. Shen, Q. Gu, F.L. Ma, L. Yip, L.T. Hou, Z.J. Qi, S.J. Su, Perovskite light-emitting diodes with EQE exceeding 28% through a synergetic dual-additive strategy for defect passivation and nanostructure regulation, Adv. Mater. 33 (2021), 2103268.
[10] L. Zhu, H. Cao, C. Xue, H. Zhang, M.C. Qin, J. Wang, K.C. Wen, Z.W. Fu, T. Jiang, L. Xu, Y. Zhang, Y. Cao, C. Tu, J. Zhang, D.W. Liu, G.B. Zhang, D.C. Kong, N. Fan, G.Q. Li, C. Yi, Q.M. Peng, J. Chang, X.H. Lu, N.N. Wang, W. Huang, J.P. Wang, Unveiling the additive-assisted oriented growth of perovskite crystallite for high performance light-emitting diodes, Nat. Commun. 12 (2021) 5081.
[11] Z.L. Yan, J.S. Benas, C.C. Chueh, W.C. Chen, F.C. Liang, Z.X. Zhang, B.H. Lin, C. J. Su, T. Chiba, J. Kido, C.C. Kuo, Stable blue perovskite light-emitting diodes achieved by optimization of crystal dimension through zinc bromide addition, Chem. Eng. J. 414 (2021), 128774.
[12] Y. Tian, X.Y. Qian, C.C. Qin, M.H. Cui, Y.Q. Li, Y.C. Ye, J.K. Wang, W.J. Wang, J. X. Tang, Modulating low-dimensional domains of self-assembling quasi-2D

perovskites for efficient and spectra-stable blue light-emitting diodes, Chem. Eng. J. 415 (2021), 129088.
[13] Z.H. Zhu, Y. Wu, Y. Shen, J.H. Tan, D. Shen, M.F. Lo, M.L. Li, Y. Yuan, J.X. Tang, W.J. Zhang, S.W. Tsang, Z.Q. Guan, C.S. Lee, Highly efficient sky-blue perovskite light-emitting diode via suppressing nonradiative energy loss, Chem. Mater. 33 (2021) 4154–4162.
[14] S. Zhang, H.L. Liu, X.G. Li, S.R. Wang, Enhancing quantum yield of $CsPb(Br_xCl_{1-x})_3$ nanocrystals through lanthanum doping for efficient blue light-emitting diodes, Nano Energy 77 (2020), 105302.
[15] F.J. Zhang, B. Cai, J.Z. Song, B.N. Han, B.S. Zhang, H.B. Zeng, Efficient blue perovskite light-emitting diodes boosted by 2D/3D energy cascade channels, Adv. Funct. Mater. 30 (2020), 2001732.
[16] F. Yuan, C.X. Ran, L. Zhang, H. Dong, B. Jiao, X. Hou, J.R. Li, Z.X. Wu, A cocktail of multiple cations in inorganic halide perovskite toward efficient and highly stable blue light-emitting diodes, ACS Energy Lett. 5 (2020) 1062–1069.
[17] F. Yang, H. Chen, R. Zhang, X. Liu, W. Zhang, J. Zhang, F. Gao, L. Wang, Efficient and spectrally stable blue perovskite light-emitting diodes based on potassium passivated nanocrystals, Adv. Funct. Mater. 30 (2020), 1908760.
[18] L. Cai, D. Liang, X.C. Wang, J.Q. Zang, G.L. Bai, Z.W. Hong, Y.T. Zou, T. Song, B. Q. Sun, Efficient and bright pure-blue all-inorganic perovskite light-emitting diodes from an ecofriendly alloy, J. Phys. Chem. Lett. 12 (2021) 1747–1753.
[19] Q. Wang, X. Wang, Z. Yang, N. Zhou, Y. Deng, J. Zhao, X. Xiao, P. Rudd, A. Moran, Y. Yan, J. Huang, Efficient sky-blue perovskite light-emitting diodes via photoluminescence enhancement, Nat. Commun. 10 (2019) 5633.
[20] H. Zhang, X. Fu, Y. Tang, H. Wang, C. Zhang, W.W. Yu, X. Wang, Y. Zhang, M. Xiao, Phase segregation due to ion migration in all-inorganic mixed-halide perovskite nanocrystals, Nat. Commun. 10 (2019) 1088.
[21] J.-P. Correa-Baena, Y. Luo, T.M. Brenner, J. Snaider, S. Sun, X. Li, M.A. Jensen, N. T.P. Hartono, L. Nienhaus, S. Wieghold, J.R. Poindexter, S. Wang, Y.S. Meng, T. Wang, B. Lai, M.V. Holt, Z. Cai, M.G. Bawendi, L. Huang, T. Buonassisi, D. P. Fenning, Homogenized halides and alkali cation segregation in alloyed organic-inorganic perovskites, Science 363 (2019) 627–631.
[22] M.C. Brennan, A. Ruth, P.V. Kamat, M. Kuno, Photoinduced anion segregation in mixed halide perovskites, Trends in Chemistry 2 (2020) 282–301.
[23] Z.W. Ren, K. Wang, X.W. Sun, W.C.H. Choy, Strategies toward efficient blue perovskite light-emitting diodes, Adv. Funct. Mater. 31 (2021), 2100516.
[24] J. Xing, Y. Zhao, M. Askerka, L.N. Quan, X. Gong, W. Zhao, J. Zhao, H. Tan, G. Long, L. Gao, Z. Yang, O. Voznyy, J. Tang, Z.-H. Lu, Q. Xiong, E.H. Sargent, Color-stable highly luminescent sky-blue perovskite light-emitting diodes, Nat. Commun. 9 (2018) 3541.
[25] Y. Zou, H. Xu, S. Li, T. Song, L. Kuai, S. Bai, F. Gao, B. Sun, Spectral-stable blue emission from moisture-treated low-dimensional lead bromide-based perovskite films, ACS Photonics 6 (2019) 1728–1735.
[26] L. Song, L. Huang, Y. Liu, Y. Hu, X. Guo, Y. Chang, C. Geng, S. Xu, Z. Zhang, Y. Zhang, N. Luan, Efficient and stable blue perovskite light-emitting devices based on inorganic Cs_4PbBr_6 spaced low-dimensional $CsPbBr_3$ through synergistic control of amino alcohols and polymer additives, ACS Appl. Mater. Interfaces 13 (2021) 33199–33208.
[27] K. Sun, Z. Bao, X. Guo, J. Ou, Y. Lv, D. Zou, L. Song, Y. Li, X. Liu, J. Liang, Pure bromide-based inorganic perovskite sky-blue light-emitting diodes through phase control by the NiO_x anode interface, J. Mater. Chem. C 10 (2022) 9538–9545.
[28] G. Li, Z.K. Tan, D. Di, M.L. Lai, L. Jiang, J.H. Lim, R.H. Friend, N.C. Greenham, Efficient light-emitting diodes based on nanocrystalline perovskite in a dielectric polymer matrix, Nano Lett. 15 (2015) 2640–2644.
[29] Y. Ling, Y. Tian, X. Wang, J.C. Wang, J.M. Knox, F. Perez-Orive, Y. Du, L. Tan, K. Hanson, B. Ma, H. Gao, Enhanced optical and electrical properties of polymer-assisted all-inorganic perovskites for light-emitting diodes, Adv. Mater. 28 (2016) 8983–8989.
[30] L. Song, X. Guo, Y. Hu, Y. Lv, J. Lin, Z. Liu, Y. Fan, X. Liu, Efficient inorganic perovskite light-emitting diodes with polyethylene glycol passivated ultrathin $CsPbBr_3$ films, J. Phys. Chem. Lett. 8 (2017) 4148–4154.
[31] Z. Li, Z. Chen, Y. Yang, Q. Xue, H.-L. Yip, Y. Cao, Modulation of recombination zone position for quasi-two-dimensional blue perovskite light-emitting diodes with efficiency exceeding 5, Nat. Commun. 10 (2019) 1027.
[32] R. Yang, Y.-Q. Li, M.-L. Guo, X.-Y. Cai, J.-X. Tang, Efficient pure-red perovskite light-emitting diodes using dual-Lewis-base molecules for interfacial modification, J. Mater. Chem. C 9 (2021) 9169–9177.
[33] Y. Bai, H. Chen, S. Xiao, Q. Xue, T. Zhang, Z. Zhu, Q. Li, C. Hu, Y. Yang, Z. Hu, F. Huang, K.S. Wong, H.-L. Yip, S. Yang, Effects of a molecular monolayer modification of NiO nanocrystal layer surfaces on perovskite crystallization and interface contact toward faster hole extraction and higher photovoltaic performance, Adv. Funct. Mater. 26 (2016) 2950–2958.
[34] J. Ou, X. Guo, L. Song, J. Lin, Y. Lv, Y. Fan, Y. Li, D. Zou, Z. Bao, X. Liu, Ampholytic interface induced in situ growth of $CsPbBr_3$ for highly efficient perovskite light-emitting diodes, J. Mater. Chem. C 9 (2021) 1025–1033.
[35] Y. Shen, H.Y. Wu, Y.Q. Li, K.C. Shen, X.Y. Gao, F. Song, J.X. Tang, Interfacial nucleation seeding for electroluminescent manipulation in blue perovskite light-emitting diodes, Adv. Funct. Mater. 31 (2021), 2103870.
[36] I. Schmidt, S. Olthof, H. Xu, K. Meerholz, Phosphine oxide additives for high-brightness inorganic perovskite light-emitting diodes, Adv. Opt. Mater. 10 (2022), 2101602.
[37] M. Yuan, Q. Li Na, R. Comin, G. Walters, R. Sabatini, O. Voznyy, S. Hoogland, Y. Zhao, E.M. Beauregard, P. Kanjanaboos, Z. Lu, D.H. Kim, E.H. Sargent, Perovskite energy funnels for efficient light-emitting diodes, Nat. Nanotechnol. 11 (2016) 872–877.
[38] J.A. Sichert, Y. Tong, N. Mutz, M. Vollmer, S. Fischer, K.Z. Milowska, R. G. Cortadella, B. Nickel, C. Cardenas-Daw, J.K. Stolarczyk, A.S. Urban, J. Feldmann, Quantum size effect in organometal halide perovskite nanoplatelets, Nano Lett. 15 (2015) 6521–6527.
[39] F. Qin, H. Tian, M. Yan, Y. Fang, D. Yang, Cesium-lead-bromide perovskites with balanced stoichiometry enabled by sodium-bromide doping for all-vacuum deposited silicon-based light-emitting diodes, J. Mater. Chem. C 9 (2021) 2016–2023.
[40] X. Liu, X. Guo, Y. Lv, Y. Hu, Y. Fan, J. Lin, X. Liu, X. Liu, High brightness and enhanced stability of $CsPbBr_3$-based perovskite light-emitting diodes by morphology and interface engineering, Adv. Opt. Mater. 6 (2018), 1801245.
[41] J.N. Li, X.C. Wang, Y.S. Tan, D. Liang, Y.T. Zou, L. Cai, T. Wu, K.C. Wen, Y.S. Wang, Y.J. Li, T. Song, L. Wang, B.Q. Sun, Strontium ion B-site substitution for spectral-stable blue emitting perovskite light-emitting diodes, Adv. Opt. Mater. 8 (2020), 2001073.
[42] S. Kang, S. Park, S. Park, H. Kwon, J. Lee, K.H. Hong, Y.J. Pu, J. Park, Achieving green and deep-blue perovskite LEDs by dimensional control using various ammonium bromides with $CsPbBr_3$, Mater, Today Energy 21 (2021), 100749.